STRUCTURAL UNCERTAINTY ESTIMATION OF TURBULENCE MODELS IN ORGANIC RANKINE CYCLE APPLICATIONS

Giulio Gori[1*], Nassim Razaaly[1], Gianluca Iaccarino[2], Pietro M. Congedo [1]

[1] DeFI Team (Inria Saclay Île-de-France, Ecole Polytechnique), CMAP Lab,
Palaiseau, Essonne, France
giulio.gori@inria.fr

[2] Department of Mechanical Engineering and Institute for Computational and Mathematical Engineering, Stanford University,
Stanford, California, U. S. A.

ABSTRACT

Nowadays, the investigation of complex fluid flows developing within Organic Rankine Cycle (ORC) turbomachines widely relies on numerical tools. In Computational Fluid Dynamics (CFD) simulations, a popular strategy consists in modeling the flow by means of the Reynolds-Averaged Navier-Stokes equations (RANS). Turbulence models must be employed to reconstruct the Reynolds stress term arising from the time-averaged decomposition of the Navier-Stokes equations. The scarce amount of experimental data prevents the correct estimation of turbulence coefficients for non-ideal flows of interest for ORC applications. Besides, the direct quantification of the errors introduced by RANS closure models is intractable in general. Recently, formal uncertainty quantification techniques have been developed to provide a probabilistic characterization of the confidence levels associated to turbulence modeling. Here, the Eigenspace Perturbation Method (EPM) is applied to a set of exemplary flow configurations of interest for ORC applications. Namely, a non-ideal flow expanding through a converging-diverging nozzle, a non-ideal supersonic stream over a backward facing step and the flow around a typical ORC turbine stator blade. Numerical results show that a systematic and comprehensive treatment of the RANS inherent uncertainties is fundamental to the further improvement and optimization of ORC power production systems.

1. INTRODUCTION

The characterization of Non-Ideal Compressible-Fluid Dynamics (NICFD) flows is of the utmost importance for Organic Rankine Cycle (ORC) applications, see Congedo et al. (2011); Wheeler and Ong (2013); Colonna et al. (2015). In the non-ideal regime, the flow may be subject to inverted thermodynamic features, see for instance Cramer and Best (1991); Schnerr and Leidner (1991); Gori et al. (2017a); Vimercati et al. (2018). Unfortunately, NICFD is still a quite unexplored field and, despite the efforts done by research groups from all over the world, a large number of questions still remains unanswered. Currently, the investigation of the non-ideal fluid flows developing within ORC turbomachines largely relies on Computational Fluid Dynamics (CFD) solvers. In CFD simulations, a popular strategy consists in solving the Reynolds-Averaged Navier-Stokes equations (RANS) which, as known, require additional thermodynamics and turbulence closures to be provided. In the past decades, challenging research endeavors yield the formulation of accurate thermodynamic models for NICFD flows, see Colonna et al. (2006); Thol et al. (2017). Nevertheless, little was achieved regarding turbulence modeling for NICFD flows and only preliminary investigations are reported in Sciacovelli et al. (2017, 2016).

The strong inherent model-form assumptions in RANS turbulence closures introduce potential accuracy limitations which generally question the credibility of CFD predictions (Duraisamy et al., 2019). In particular, the accuracy of RANS simulations is usually poor when predicting flows involving adverse pressure gradients, non-homogeneity, separation or strong stream lines curvature like the ones concerning turbomachinery applications. Tough literature is teemed with works reporting on turbulence modeling concerning flows of fluids of common interest (i.e., air or water), little, if nothing, can be found about

ORC applications. Unfortunately, due to the high complexity of turbulence phenomena and due to the large number of unknowns involved, the direct quantification of the errors introduced by RANS closure models is intractable in general. Nevertheless, RANS simulations are currently considered as one of the most powerful tool researchers may use to investigate NICFD flows and to design machinery operating with fluids in the non-ideal regime.

Recently, formal uncertainty quantification techniques have been developed to provide a probabilistic characterization of the confidence levels corresponding to turbulence modeling approximations. In this paper, an application of the Eigenspace Perturbation Method (EPM) (Emory et al., 2013) to a set of exemplary flow configurations of interest for ORC applications is presented. The EPM is implemented within the EQUiPS library (Mishra et al., 2018) which is available through the SU2 open-source suite (Palacios et al., 2013). Note that SU2 is also equipped with a computational NICFD solver (Vitale et al., 2015; Gori et al., 2017b) which, together with EPM capabilities, makes it an unparalleled choice in the quantification of turbulence uncertainty for non-ideal compressible-fluid flows.

The SU2 suite is employed to compute the turbulence uncertainty estimates of Quantities of Interest (QoI) for ORC applications. The considered test cases involve flows of siloxane MDM (Octamethyltrisiloxane, $C_8H_{24}O_2Si_3$) vapor. Namely, a non-ideal flow expanding through a converging-diverging planar nozzle, a non-ideal supersonic stream over a backward facing step and the flow around a typical ORC turbine stator blade. Numerical results show that a systematic and comprehensive treatment of the RANS inherent uncertainties is fundamental for the further improvement and optimization of ORC power production systems.

The paper is structured as follows: Sec. 2 briefly describes the EPM, Sec. 3 presents the test cases for which the numerical uncertainty estimates are provided and Sec. 4 briefly summarizes the findings.

2. METHODOLOGY

The EPM (Emory et al., 2013) was developed to quantify the L2 (Duraisamy et al., 2019) uncertainties in RANS models. Namely, the approach relies on the eigen-decomposition of the Reynolds stress tensor to express turbulence uncertainties by means of intervals computed by perturbing the eigenspace. The EPM can be straightforwardly applied to any turbulence model. Nevertheless, in the following an eddy-viscosity based model, the Menter's Shear Stress Transport (SST) model (Menter, 1993), is employed to introduce the mathematical formulation of the EPM. The eddy viscosity scalar ν_T is computed by means of the turbulence closure, see Wilcox (1998). As pointed out in Edeling et al. (2014), each closure is subject to uncertainties on its mathematical form and on its coefficients which ultimately lead to an uncertainty on the value of the eddy viscosity. The stress tensor can be approximated as

$$\langle u_i u_j \rangle \approx \langle u_i u_j \rangle^{(bl)} = \frac{2}{3} k \delta_{ij} - 2\nu_T S_{ij}, \tag{1}$$

where k is the turbulent kinetic energy, δ_{ij} the Kronecker delta and S_{ij} is the deviatoric part of the strain-rate tensor. Note that the superscript (bl) points out the baseline stress tensor i.e., the tensor reconstructed using the selected turbulence closure, stressing the fact that $\langle u_i u_j \rangle^{(bl)}$ is just an approximation of $\langle u_i u_j \rangle$. Nevertheless, in the following the superscript (bl) is dropped to simplify the notation as we will always refer to the approximated tensor. As known, the Reynolds stress tensor $\langle u_i u_j \rangle$ can be decomposed into the anisotropic and deviatoric components yielding

$$\langle u_i u_j \rangle = 2k \left(b_{ij} + \frac{\delta_{ij}}{3} \right). \tag{2}$$

The anisotropy Reynolds stress tensor b_{ij} can be expressed in the spectral form

$$b_{ij} = v_{ik} \Lambda_{kl} v_{jl}. \tag{3}$$

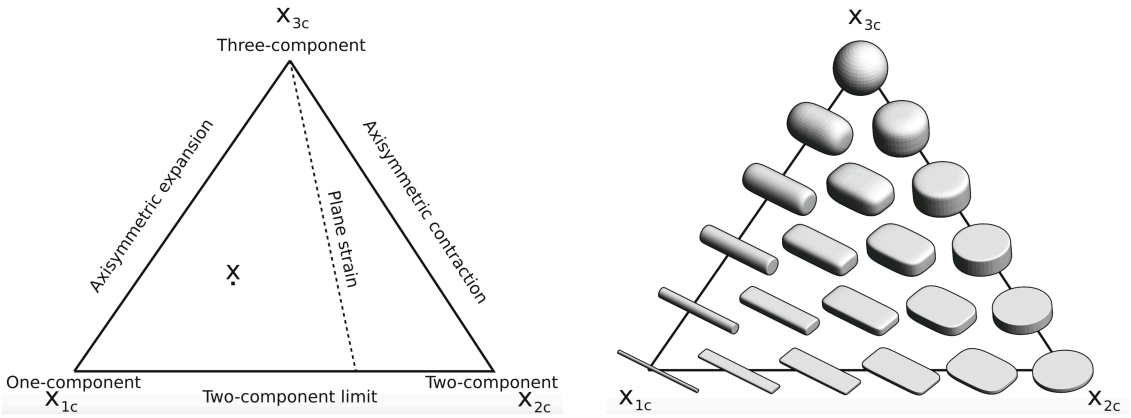

Figure 1: (a) Barycentric map of the eigenvalues in the Euclidean space; (b) The shape of the ellipsoid associated to the Reynolds stress tensor for different eigenvalues perturbations (Jofre et al., 2019).

In (3), v_{ik} and v_{jl} are the left and the right eigenvectors whereas Λ_{kl} is a diagonal matrix containing the eigenvalues ($Diag(\lambda_i)$) ordered such that $\lambda_1 \geq \lambda_2 \geq \lambda_3$.

The EPM consists in perturbing the eigenvalues and eigenvectors of the anisotropy tensor during the CFD solution iterations. The resulting tensor is expressed as

$$\left\langle u_i u_j \right\rangle^* = 2k\left(v_{ik}^* \Lambda_{kl}^* v_{jl}^* + \frac{\delta_{ij}}{3}\right), \tag{4}$$

where the superscript * refers to the perturbed entities. Perturbations allow to account for errors due to closure assumptions and they are performed in two different ways. Namely, by varying the componentiality of the flow i.e., by changing the eigenvalues, or by changing the orientation of the eigenvectors. Note that, in this work, a perturbation of the turbulent kinetic energy k is not considered.

According to Banerjee et al. (2007), since any anisotropy state corresponds to a convex combination of the limiting states of componentiality, it is possible to map the eigenvalues (λ_1, λ_2, λ_3) on a Barycentric reference frame

$$\mathbf{x} = \mathbf{x}_{1C}\left(\lambda_1 - \lambda_2\right) + 2\mathbf{x}_{2C}\left(\lambda_2 - \lambda_3\right) + \mathbf{x}_{3C}\left(3\lambda_3 + 1\right). \tag{5}$$

In an Euclidean space, the three states ($\mathbf{x}_{1C}$, $\mathbf{x}_{2C}$, $\mathbf{x}_{3C}$) correspond to the vertexes of an equilateral triangle (Jofre et al., 2019) which allows for a convenient representation of the turbulence bounds in a two-dimensional coordinate system, see Fig. 1(a). Figure 1(b) reports the graphical representation of the ellipsoid associated to the anisotropy tensor at different points on the barycentric map.

In the EPM, a perturbation is first applied to the anisotropy tensor eigenvalues so that the barycentric coordinate is moved to one limiting states of componentiality ($\mathbf{x}_{1C}$, $\mathbf{x}_{2C}$, $\mathbf{x}_{3C}$) i.e., one of the three vertexes of the triangle. After, a perturbation is applied to vary the alignment of the anisotropy tensor eigenvectors w.r.t. the principal axes of the mean rate of strain tensor $\nabla\mathbf{v}$ (being $\mathbf{v}$ the flow velocity vector). Namely, perturbing the eigenvectors corresponds to modulating the production of turbulent kinetic energy. By recalling the Frobenius inner product, $\mathcal{F} \doteq \langle A, B\rangle_{\mathrm{F}} = tr\left(A^{\mathrm{H}}B\right)$ where A and B are two matrices of same dimensions and superscript H points out the complex conjugate, it is possible to identify two limiting conditions $\mathcal{F}^{max}$ and $\mathcal{F}^{min}$ of $\langle b_{ij}, \nabla\mathbf{v}\rangle_{\mathrm{F}}$ corresponding to the maximization and the minimization of the turbulent kinetic energy production, see Iaccarino et al. (2017). Summarizing, one would need to run six different and independent CFD simulations, to compute the solution corresponding to any possible combination of the eigenvalues and eigenvectors perturbations identified above. In practice, in $\mathbf{x}_{3C}$ the ellipsoid related to the Reynolds stress tensor degenerates into a sphere which is invariant to eigenvector perturbations. This reduces the effective number of simulations to five: $\mathcal{F}_{1C}^{max}$, $\mathcal{F}_{1C}^{min}$, $\mathcal{F}_{2C}^{max}$, $\mathcal{F}_{2C}^{min}$ and $3C$.

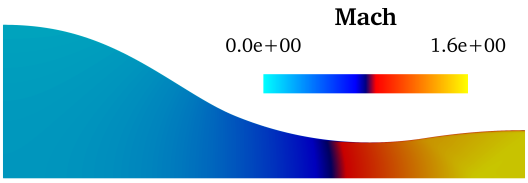

Figure 2: planar de Laval nozzle. Mach number field computed using the baseline closure.

Once the simulations are carried out, it is possible to estimate the turbulent uncertainty estimates of a QoI by extracting the max/min values among the five solutions.

One of the most interesting features of the EPM is that the framework is model agnostic and hence it can be applied regardless of the turbulence closure used to compute the baseline Reynolds Stress tensor. Since our knowledge of turbulence in the non-ideal regime is currently very limited, so is the applicability of standard turbulence models like the SST closure. For this reasons, the fact that the EPM is model agnostic makes it a perfect tool for investigating NICFD flows.

3. RESULTS

The EPM is applied to three typical domain configurations of relevant interest for ORC applications. All the considered cases involve a MDM vapor flow and the Peng-Robinson equation of state (Peng and Robinson, 1976) is used to model the non-ideal thermodynamics.

3.1 Planar de Laval nozzle

This test case involves a MDM vapor flow expanding at non-ideal conditions across a planar converging-diverging nozzle. Figure 2 reports the Mach number field computed using the baseline Reynolds stresses. The fluid flows from left to right, a symmetry condition applies at the centerline whereas the upper boundary corresponds to a solid wall. The domain is dicretised using an in-house meshing tool which implements an advancing-front/Delaunay algorithm to generate hybrid unstructured grids of triangular and quadrilateral (at walls) elements. The height of the first cell at solid walls is in the order of $1 \cdot 10^{-6}$ m, comparable to $y^+ = 1$. The y^+ is estimated using the value of viscosity returned by the FluidProp (Colonna et al., 2005) software, considering the inflow conditions, total pressure of 4.6 bar and total temperature of 512.5 K, and considering the design flow speed at the nozzle throat. In this test case, the QoI corresponds to the pressure distribution extracted along nozzle centerline. CFD simulations are marched forward in time using an implicit Euler scheme until a steady state is reached. Simulation convergence is assessed by ensuring that the pressure and drag coefficients over the curved profile reached a stable value up to the 5th decimal digit. A second-order accurate MUSCL scheme of Roe type is employed with the Venkatakrishnan flux limiting function. Thermal conductivity and viscosity are considered homogeneous scalars and are computed at the inflow nominal conditions.

First, a grid sensitivity analysis is carried out considering grid A (36k points), grid B (129k points), grid C (257k points) and grid D (500k points). The QoIs, as computed from each grid, are compared in Fig. 3(a). The comparison shows no significant difference between the targeted QoI predicted using different grids. Figure 3(b) reports the pressure absolute error associated to grid A, B and C (computed w.r.t. the solution from grid D) which is very limited and always smaller than 0.5%. Nevertheless, the five EPM simulations are run for all the four grids, to provide an assessment of the sensitivity of the turbulence uncertainty estimates to the resolution of the mesh. The max/min pressure envelope from the five EPM solutions is reconstructed for each grid. Figure 3(c) reports a comparison of the computed uncertainty estimates in the region of the nozzle discharge section, where the uncertainties due to turbulence are not negligible. Notably, even though the discretization error on the QoI obtained from the baseline turbulence model was limited for all grids (Fig. 3(a)), the uncertainty estimates are subject to a higher

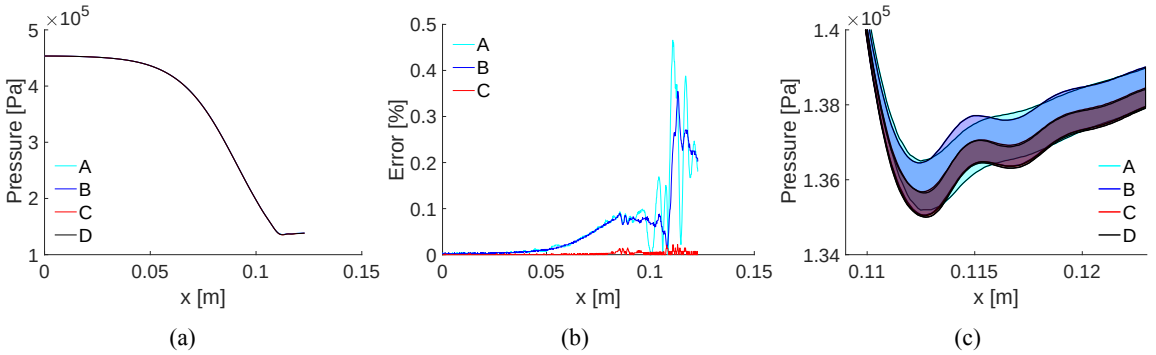

(a) (b) (c)

Figure 3: (a) Grid sensitivity analysis, pressure distribution comparison ; (b) Grid sensitivity analysis, absolute error; (c) Turbulence uncertainty estimates related to different grids.

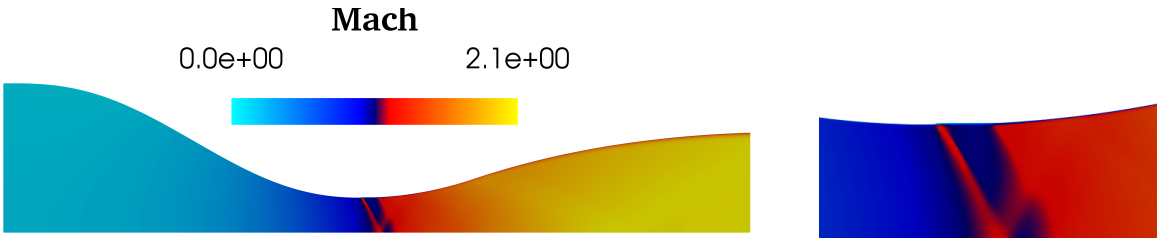

(a) (b)

Figure 4: (a) Mach number field relative to a non-ideal supersonic stream over a recessed step; (b) Enlargement of the throat region.

variability. Moreover, the integration of the pressure distribution along the upper nozzle profile returns the fluid dynamics force acting on the geometry. Namely, the vertical and the horizontal component of the aerodynamic force acting on the semi-channel are computed. Results show that there is a variability of about 0.19% and 6.37%, respectively. This was somehow expected since the vertical force is generated by a reduction of pressure due to flow acceleration. The latter is a purely inviscid phenomenon as long as there is no separation and the boundary layer has a negligible thickness. On the other hand, the horizontal component of the aerodynamic force is utterly related to the friction generated at walls i.e., it strongly depends on the turbulence model.

3.2 Supersonic flow over a recessed step

This test case consists of a non-ideal supersonic stream over a recessed step of height equal to $1 \cdot 10^{-4}$ m, see Fig. 4. The grid, which counts 537k points, was properly selected after a sensitivity study (not reported) and guarantees a resolution sufficient to resolve the boundary layer gradients. The siloxane MDM vapor flows into a converging-diverging nozzle across which it accelerates up to a supersonic speed. At the nozzle throat, a backward facing step causes the separation of the flow and the formation of a small re-circulation region. As the supersonic stream reattaches past the circulating bubble, a shock wave is formed. The shock propagates downstream into the divergent and it reflects at the centerline producing pressure fluctuations. Figure 4 reports the baseline Mach number field corresponding to an inflow total pressure of 4.6 bar and total temperature of 520 K. Thermal conductivity and viscosity are assumed homogeneous scalars and are computed at the inflow nominal conditions using the FluidProp library. Once again, an implicit Euler scheme is employed together with a second-order accurate MUSCL scheme of HLLC type limited by the Venkatakrishnan function. With reference to Fig. 4(a) and (b), a shock of finite intensity is clearly visible in the throat region. The shock produces fluctuations in flow properties, as evident in Fig. 5(a) which reports the pressure distribution along the nozzle centerline.

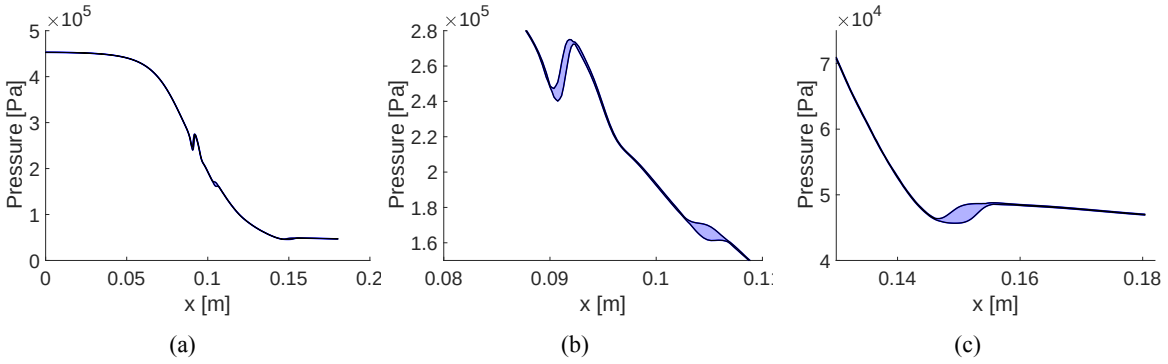

Figure 5: Non-Ideal supersonic flow over a recessed step: pressure turbulence uncertainty estimates. (a) Full domain; (b) Throat region enlargement; (c) Discharge section enlargement.

Figure 5(b) and (c) report enlargements of the pressure envelope computed using the EPM. Remarkably, the EPM returns an envelope which, in the close proximity of $x = 0.09$ m, has a maximum range of almost 20k Pa. Closure model-form uncertainties play a key role since the shape and the dimensions of the recirculating bubble and, therefore the slope of the shock, largely depend on turbulent dynamics.

3.3 ORC stator blade

This latter test case aims at evaluating the turbulence uncertainty estimates related to the non-ideal flow of siloxane MDM vapor around a typical ORC stator blade. Figure 6(a) reports the Mach number flowfield as computed using the baseline closure. At the trailing edge, the so-called fish-tail shock pattern is formed, see Vimercati et al. (2017); Galiana et al. (2017). In a cascade, shocks originated at the trailing edge propagate into the domain and interact with the boundary layer developing over the pressure side of the neighboring blade. In the light of this facts, it is clear that structural uncertainty in turbulence models results into an uncertainty over the predicted blade performances. Here, the EPM is applied to investigate the variability of the total pressure loss across the cascade and of the skin friction coefficient over the blade surface. Again, a grid sensitivity analysis led to the selection of a two-dimensional periodic grid composed by 590k points. Simulations were run using a second-order accurate MUSCL scheme of Roe type coupled to the Van Albada limiter. Inflow fluid conditions correspond to a total pressure of 8 bar and a total temperature 545 K. At the outflow, a non-reflective BC applies a static pressure of 1 bar. The EPM returns an interval of values for the total pressure loss, computed as a percentage w.r.t. the nominal inflow, which spans from a maximum of 20.3% to a minimum of 17%. That is, the structural uncertainties yield a potential variability of about 19% on the computed total pressure losses. Moreover, the maximum and the minimum kinetic energy loss are, respectively, 7.99% and 6.58% with a variability of about 21.5%. On the other hand, the turbulence estimates on the outlet flow angle are negligible. Figure 6(b) reports the skin friction coefficient ($C_f = 2\tau_w/\rho u^2$, being τ_w the skin shear stress on the surface, ρ the density of the fluid and u the free stream speed) as computed along the blade pressure and suction sides. Clearly, the magnitude and the orientation of the skin shear stresses are strictly related to the turbulence closure, thus suffering from a great variability w.r.t. the structural uncertainties.

4. CONCLUSIONS

The Eigenspace Perturbation Method is applied to compute the model-form turbulence uncertainty estimates of several quantities of interest in flow configurations relevant to Organic Rankine Cycle applications. The EPM framework provides five distinct limiting states of turbulence componentiality/orientation that are used to evaluate approximate bounds of QoIs due to model-form uncertainty of the Reynolds stress tensor. In the paper, model-form uncertainties are shown to be particularly relevant to ORC turbomachinery applications since the flow-field developing around a typical blade is usually characterized

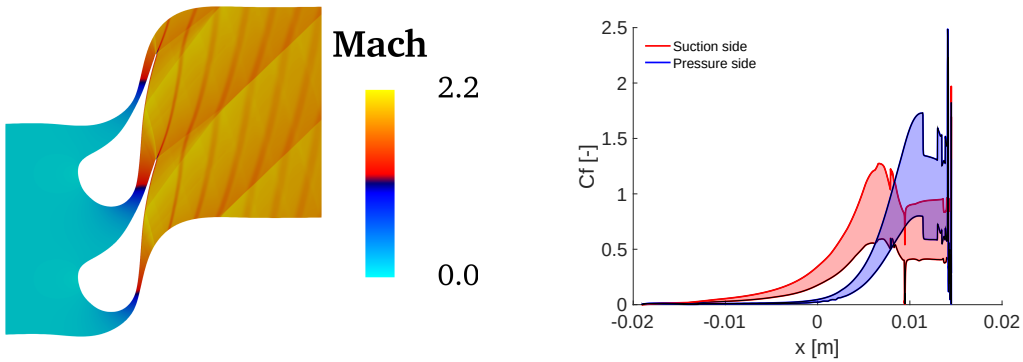

(a) (b)

Figure 6: (a) Mach number field around a typical ORC turbine stator blade computed using the baseline Reynolds stresses; (b) Skin friction coefficient turbulence uncertainty estimates.

by a broad set of viscous phenomena. Indeed, it is shown that the targeted QoIs, in particular turbine performances, suffer from a significantly large variability related to turbulence closure uncertainty. In this perspective, the credibility of deterministic RANS-based approaches for the investigation and the optimization of NICFD applications is at least questionable. In other words, advanced Uncertainty Quantification techniques must be employed to investigate and optimize the performances of ORC turbines. The scarce knowledge regarding the development of turbulent structures in NICFD flows pave the road for a novel, and possibly prolific, research front which spans from the development of robust optimization techniques accounting for turbulence model-form uncertainties to experimental investigations.

REFERENCES

Banerjee, S., Krahl, R., Durst, F., and Zenger, C. (2007). Presentation of anisotropy properties of turbulence, invariants versus eigenvalue approaches. *Journal of Turbulence*, 8.

Colonna, P., Casati, E., Trapp, C., Mathijssen, T., Larjola, J., Turunen-Saaresti, T., and Uusitalo, A. (2015). Organic Rankine Cycle power systems: From the concept to current technology, applications, and an outlook to the future. *J. Eng. Gas Turb. Power*, 137(10).

Colonna, P., der Stelt, T. P., and Guardone, A. (2005). FluidProp: A program for the estimation of thermophysical properties of fluids. Energy Technology Section, TU Delft, The Netherlands.

Colonna, P., Nannan, N. R., Guardone, A., and Lemmon, E. W. (2006). Multiparameter equations of state for selected siloxanes. *Fluid Phase Equilib.*, 244(2):193–211.

Congedo, P., Corre, C., and Cinnella, P. (2011). Numerical investigation of dense-gas effects in turbomachinery. *Comput. & Fluids*, 49(1):290–301.

Cramer, M. S. and Best, L. M. (1991). Steady, isentropic flows of dense gases. *Phys. Fluids A*, 3(4).

Duraisamy, K., Iaccarino, G., and Xiao, H. (2019). Turbulence modeling in the age of data. *Annual Review of Fluid Mechanics*, 51.

Edeling, W., Cinnella, P., Dwight, R., and Bijl, H. (2014). Bayesian estimates of parameter variability in the k − ε turbulence model. *Journal of Computational Physics*, 258:73–94.

Emory, M., Larsson, J., and Iaccarino, G. (2013). Modeling of structural uncertainties in reynolds-averaged navier-stokes closures. *Physics of Fluids*, 25(11):110822.

Galiana, F. J. D., Wheeler, A. P. S., Ong, J., and de M. Ventura, C. A. (2017). The effect of dense gas dynamics on loss in ORC transonic turbines. *Journal of Physics: Conference Series*, 821(1):012021.

Gori, G., Vimercati, D., and Guardone, A. (2017a). Non-ideal compressible-fluid effects in oblique shock waves. *Journal of Physics: Conference Series*, 821(1):012003.

Gori, G., Zocca, M., Cammi, G., Spinelli, A., and Guardone, A. (2017b). Experimental assessment of the open-source SU2 CFD suite for ORC applications. *Energy Procedia*, 129(Supplement C):256–263.

Iaccarino, G., Mishra, A., and Ghili, S. (2017). Eigenspace perturbations for uncertainty estimation of single-point turbulence closures. *Physical Review Fluids*, 2.

Jofre, L., Domino, S., and Iaccarino, G. (2019). Characterization of structural uncertainty in les of a round jet. pages 137–150.

Menter, F. (1993). Zonal two equation $k - \omega$, turbulence models for aerodynamic flows. *AIAA Paper*.

Mishra, A., Mukhopadhaya, J., Iaccarino, G., and Alonso, J. J. (2018). An uncertainty estimation module for turbulence model predictions in SU2. *AIAA Journal*.

Palacios, F., Alonso, J. J., Duraisamy, K., Colonno, M., Hicken, J., Aranake, A., Campos, A., Copeland, S., Economon, T. D., Lonkar, A., Lukaczyk, T., and Taylor, T. (2013). Stanford University Unstructured (SU^2): An open-source integrated computational environment for multi-physics simulation and design. *AIAA Paper 2013-0287*.

Peng, D. Y. and Robinson, D. B. (1976). A new two-constant equation of state. *Ind. Eng. Chem. Fundam.*

Schnerr, G. H. and Leidner, P. (1991). Diabatic supersonic flows of dense gases. *Phys. Fluids A*, 3(10):2445–2458.

Sciacovelli, L., Cinnella, P., Content, C., and Grasso, F. (2016). Dense gas effects in inviscid homogeneous isotropic turbulence. *Journal of Fluid Mechanics*, 800:140?179.

Sciacovelli, L., Cinnella, P., and Grasso, F. (2017). Small-scale dynamics of dense gas compressible homogeneous isotropic turbulence. *Journal of Fluid Mechanics*, 825:515?549.

Thol, M., Dubberke, F. H., Baumhogger, E., Vrabec, J., and Span, R. (2017). Speed of sound measurements and fundamental equations of state for octamethyltrisiloxane and decamethyltetrasiloxane. *Journal of Chemical & Engineering Data*, 62(9):2633–2648.

Vimercati, D., Gori, G., and Guardone, A. (2018). Non-ideal oblique shock waves. *Journal of Fluid Mechanics*, 847:266–285.

Vimercati, D., Gori, G., Spinelli, A., and Guardone, A. (2017). Non-ideal effects on the typical trailing edge shock pattern of ORC turbine blades. *Energy Procedia*, 129(Supplement C):1109–1116.

Vitale, S., Gori, G., Pini, M., Guardone, A., Economon, T. D., Palacios, F., Alonso, J. J., and Colonna, P. (2015). Extension of the SU2 open source CFD code to the simulation of turbulent flows of fluids modelled with complex thermophysical laws. Number AIAA Paper 2015-2760.

Wheeler, A. and Ong, J. (2013). The role of dense gas dynamics on organic rankine cycle turbine performance. *J. Eng. Gas Turbines Power*, 135(10):102603.

Wilcox, D. (1998). *Turbulence Modeling for CFD*. 2nd Ed., DCW Industries, Inc.

ACKNOWLEDGEMENT

This research was funded by the UTOPIAE Marie Curie Innovative Training Network, H2020-MSCA-ITN-2016, Grant Agreement number 722734.